

Diameter-Dependent Electromechanical Properties of GaN Nanowires

Chang-Yong Nam,^{†,§} Papot Jaroenapibal,^{†,§} Douglas Tham,[†] David E. Luzzi,[†] Stephane Evoy,^{*,‡} and John E. Fischer^{*,†}

Department of Materials Science and Engineering, University of Pennsylvania, 3231 Walnut Street, Philadelphia, Pennsylvania 19104-6272, and Department of Electrical and Computer Engineering & National Institute for Nanotechnology, University of Alberta, ECERF W2-085, Edmonton, Alberta T6G 2V4, Canada

Received September 16, 2005; Revised Manuscript Received November 12, 2005

ABSTRACT

The diameter-dependent Young's modulus, E , and quality factor, Q , of GaN nanowires were measured using electromechanical resonance analysis in a transmission electron microscope. E is close to the theoretical bulk value (~ 300 GPa) for a large diameter nanowire ($d = 84$ nm) but is significantly smaller for smaller diameters. At room temperature, Q is as high as 2800 for $d = 84$ nm, significantly greater than what is obtained from micromachined Si resonators of comparable surface-to-volume ratio. This implies significant advantages of smooth-surfaced GaN nanowire resonators for nanoelectromechanical system (NEMS) applications. Two closely spaced resonances are observed and attributed to the low-symmetry triangular cross section of the nanowires.

Gallium nitride (GaN) is an important wide- and direct- band gap semiconductor for photonic and high-power devices.^{1,2} Bulk GaN possesses excellent thermal stability,³ chemical inertness,⁴ and a high piezoelectric constant,⁵ making it suitable for high-temperature chemical sensors and transducers. One-dimensional (1D) GaN nanowires have also attracted extensive research interest for their enhanced physical properties^{6,7} and nanoscale device applications.^{8–12} Nanomachining now allows the fabrication of mechanical objects with lateral dimensions reaching 20 nm and resonant frequencies in the ultrahigh frequency (UHF) range. Given their small volumes and high surface-to-volume ratio, these nanoelectromechanical systems (NEMS) are of great interest for the detection of masses with high sensitivity. However, conventional top-down fabrication imposes performance limits from lithographic resolution, etch roughness, and thin film growth techniques.¹³ Small-diameter, straight GaN nanowires with naturally smooth surfaces would therefore provide an interesting alternative for the production of NEMS devices. The electromechanical properties of such structures remain relatively unexplored.

Measuring the mechanical properties of individual nanowires by conventional techniques is not trivial. Optical measurements used commonly in microelectromechanical systems (MEMS) are not readily applicable to nanowire resonators because the diameter is less than a visible

wavelength. Atomic force microscopy (AFM) has been used to measure the Young's modulus, E , of an individual SiC nanorod.¹⁴ Alternatively, transmission electron microscopy (TEM) permits direct and quantitative determination of mechanical resonances by applying an actuating signal between the nanostructure and a counter-electrode. Elastic beam theory can then be employed to relate the observed resonance frequency to E . This approach has been applied successfully to carbon nanotubes,^{15,16} peapods,¹⁷ and other nanowire/nanobelt systems.¹⁸

In this letter we report the diameter-dependent E and quality factor Q of GaN nanowires by performing in situ detection of electromechanical resonances in the TEM. For the largest nanowire diameter studied ($d = 84$ nm), E is close to the theoretical value of bulk GaN (~ 300 GPa)^{19,20} and decreases gradually for smaller diameters. Also, we find $Q \approx 2800$ despite the large surface-to-volume ratio. Many samples exhibit two closely spaced resonances, which we attribute to cross sections observed in TEM that exhibit small deviations from equilateral triangles.

Wurtzite structure GaN nanowires were grown on Si substrates by thermal reaction of Ga₂O₃ and NH₃ via the vapor–liquid–solid mechanism using an Au/Pd catalyst.^{21,22} Diameters ranged from 30 to 150 nm, with lengths varying from 5 to 30 μm . Extensive electron diffraction experiments showed that the dominant growth orientation was [120], for which we expect and observe isosceles triangular cross sections (Figure 1a) with ($\bar{2}1\bar{2}$), ($2\bar{1}\bar{2}$), and (001) facets as depicted in Figure 1b.

* Corresponding authors. E-mail: fischer@seas.upenn.edu; evoy@ece.ualberta.ca.

[†] University of Pennsylvania.

[‡] University of Alberta.

[§] The authors made equal contribution in this study.

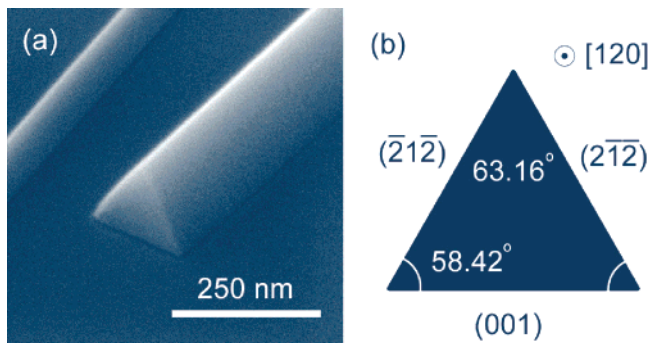


Figure 1. (a) SEM image revealing triangular cross sections of a GaN nanowire at a broken end. All directions and planes identified from electron diffraction. (b) Schematic diagram of a [120]-axis nanowire with lattice constants of wurtzite GaN. The cross section is an isosceles rather than equilateral triangle because the c/a ratio does not correspond to close-packing. The cross-sectional area is 1.4% smaller than that of an equilateral triangle with the same base length (opposite of the 63° apex).

Electromechanical resonances were characterized in a JEOL 2010 TEM operating at 200 kV. A cluster of nanowires was transferred from the growth substrate to an electrochemically sharpened tungsten tip and affixed with silver paint. The tip was then loaded onto a custom-built TEM specimen holder¹⁶ with electrical connections to the tip and a counter-electrode. A 3–10 V sine wave was applied between the tip and the counter electrode using a Stanford Research System DS430 signal generator. Resonances were detected in situ by manually tuning the frequency until the maximum vibration amplitude was observed. In selected experiments, a series of images at various frequencies near the resonance were acquired using a charge-coupled-device (CCD) camera, and the amplitude versus frequency was analyzed to evaluate the resonance quality factor, Q . Length L and “diameter” d were determined directly from their projections in TEM micrographs after carefully adjusting the sample tilt to obtain maximal values. For L this means tilting the nanowire axis normal to the beam axis. We take the diameter, d , to be the base of the approximately equilateral triangle, determined by observing thickness contrast as a function of tilt to ensure that one of the triangular facets was perpendicular to the electron beam.

Figure 2 shows a typical TEM image of a GaN nanowire driven at the resonant frequency, along with the corresponding amplitude versus frequency, f , plot. The absence of nodes indicates that the nanowire is being driven at the fundamental resonance, f_0 (Figure 2a); we never observed higher harmonics. The data in Figure 2b are well represented by a least-squares fit to a Lorentzian, indicating that the amplitude was sufficiently small that the restoring force varied linearly with displacement. We define Q as the center frequency divided by the full-width-at-half-maximum (fwhm); the fit yields $Q \approx 2800$ for the $d = 84$ nm diameter nanowire. This value is substantially higher than those reported in other studies of nanotube electromechanical resonators of similar dimensions.¹⁵

According to the Euler–Bernoulli analysis of a cantilevered beam, the resonance frequency, f_0 , depends on the

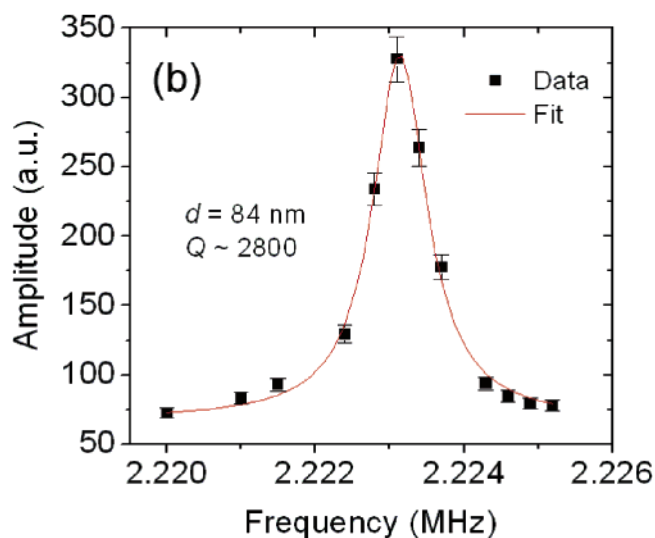
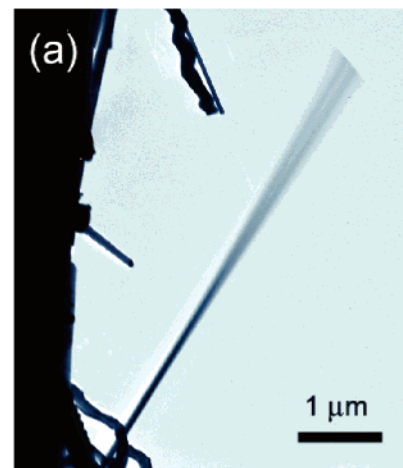


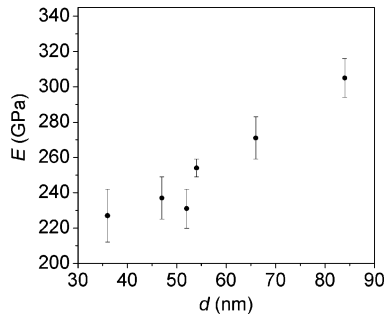
Figure 2. (a) Low-magnification TEM image of a $d = 84$ nm diameter GaN nanowire in the fundamental resonance, 2.223 MHz. (b) Amplitude vs frequency from CCD images, fit to a Lorentzian; the quality factor, Q , is 2800.

unique intensive material parameter, E , according to $f_0 = B_1^2/2\pi L^2\sqrt{EI/\rho A}$, where $B_1 = 1.875$ for the first harmonic, L , A , and ρ are the length, cross-sectional area, and mass density of the beam, and E and I are the Young’s modulus and moment of inertia, respectively.²³ For equilateral triangular cross-section beams $A = \sqrt{3}d^2/4$ and $I = \sqrt{3}d^4/96$ to yield $f_0 = B_1^2/2\pi L^2\sqrt{Ed^2/24\rho}$. For arbitrary cross sections I , the second moment of A has two orthogonal components and therefore two fundamental resonances are present. Young’s modulus, E , the ratio of stress to strain on the load plane along the load direction in uniaxial tension, is a scalar property that depends on the components of the elastic stiffness or compliance tensor; thus, E will be different for tension along different crystal directions. The current experiment measures E along the growth direction, the wurtzite [120]. Transverse shear deformation is negligible if the aspect ratio is larger than ~ 100 for anisotropic materials.²⁴ Aspect ratios in this work ranged from 65 to 200, and the amplitude at resonance was maintained below $L/10$ to minimize the bending curvature and satisfy the assumptions behind the Euler–Bernoulli equation.

Table 1. Measured Dimensions, Resonance Frequency, Young's Modulus, and Quality Factor of GaN Nanowires^a

no.	diameter d (nm, ± 2 nm)	length L (μm , $\pm 0.05 \mu\text{m}$)	fundamental resonance frequency f_0			Young's modulus E (GPa)	quality factor Q
			f_0 (MHz)	f'_0 (MHz)	f_0/f'_0		
1	84	5.5	2.235	2.223	1.005	305 ± 11	2800 ± 100
2	66	4.7	2.264		(1.000)	271 ± 12	
3	54	11.2	0.316		(1.000)	254 ± 5	1700 ± 300
4	52	4.3	1.925	1.860	1.035	231 ± 10	2300 ± 200
5	47	3.95	2.135		(1.000)	237 ± 12	500 ± 100
6	36	3.2	2.440	2.194	1.112	227 ± 15	

^a f'_0 denotes the second close fundamental resonance frequency. Estimated errors on E are dominated by uncertainties in L .

**Figure 3.** Young's modulus E vs d from Euler–Bernoulli analysis of resonance frequencies.

Returning to Figure 2, and taking for ρ the density of bulk GaN, 6.15 g/cm^3 , we find $E = 305 \text{ GPa}$ for this rather large nanowire, very close to the theoretical E of bulk GaN, $\sim 300 \text{ GPa}$,^{19,20} and to values measured for an epitaxial film and a single crystal.^{25–27} We measured E from six nanowires with different d and L and determined Q for four of them. Dimensions, f_0 , E , and Q are listed in Table 1. Figure 3 shows the dependence of E on d ; E decreases from ~ 300 to $\sim 220 \text{ GPa}$ as d decreases from 84 to 36 nm. We also found Q values ranging from ~ 500 to 2800.

The decrease of E with decreasing diameter is somewhat unexpected. For single-crystal materials, E is expected to rather increase with decreasing crystal size because the probability of finding a defect decreases as the size becomes smaller than the mean spacing between defects. This has been observed in microwhiskers,²⁸ and a recent experiment in SiC nanorods showed that E approaches the theoretical value when d is reduced to $\sim 20 \text{ nm}$.¹⁴ One possible explanation for the converse behavior is the increase of surface-to-volume ratio (S/V) with decreasing d ; the atomic coordination and cohesion near the surface are “poor” relative to bulk, and the increasing dominance of the surface would decrease the rigidity of the structure.²⁹ Recent atomic simulation results for W ³⁰, Ni ³¹, and SiSe_2 ³² nanowires consistently demonstrate E decreasing with decreasing d , although the d was an order of magnitude or more smaller than that in our experiments. Another possibility might be related to defects that exist in our GaN nanowires. In fact, high-resolution TEM imaging of similar wires reveals (001) stacking faults running parallel to the nanowire axis; some atomic layers consist of bands of cubic GaN layers within the predominantly wurtzite GaN matrix.³³ These faults might provide mechanical instability

in the crystal especially when bending-induced shear force is acting parallel to the fault planes. However, we cannot explain the trend of decreasing E with decreasing d unless the density of defects is also dependent on d .

The inverse factor $1/Q$ is related to energy dissipation, which can be extrinsic and/or intrinsic. For instance, if a resonator is operating in air, dissipation arises primarily from air damping, an extrinsic effect.³⁴ The present experiment was performed in $\sim 10^{-7}$ Torr, so we only need to consider intrinsic mechanisms such as “internal friction” involving surfaces or structural defects. Carr et al. showed that in micromachined single-crystalline Si nanowire resonators, Q decreases from ~ 3000 to ~ 1000 as S/V increases from 0.02 to 0.06 nm^{-1} (equivalent to decreasing d).³⁵ The Q values reported here are considered as lower bounds. Because we cannot visualize the clamped end in the microscope, the instantaneous beam profile may not satisfy the Euler–Bernoulli condition; in particular, the assumption of perfect clamping may not apply. The known presence of stacking defects and cubic intergrowths will also limit Q . However, it is important to note that the GaN nanowire resonator described here exhibits higher Q than that of micromachined Si resonators for the same S/A , suggesting lower surface-related energy dissipation. The Q value of our GaN resonators is as high as ~ 2800 at $S/V = 0.08 \text{ nm}^{-1}$ and still ~ 2000 at $S/V = 0.13 \text{ nm}^{-1}$. This demonstrates an important advantage of intrinsically smooth-surfaced GaN nanowires for NEMS applications compared to conventionally fabricated Si devices or Si nanowires grown by chemical vapor deposition. The latter are expected to exhibit more surface losses either because of etch roughness (top down) or surface oxide layers (bottom up).

Three out of six nanowires showed two closely spaced resonant frequencies (Table 1) corresponding to oscillatory motion in two orthogonal planes (Figure 4). The ratio of the two frequencies ranged from 1.005 to 1.112 as listed in Table 1. A similar phenomenon was observed in ZnO nanobelts.³⁶ In both cases the existence of two normal modes can be attributed to the low-symmetry cross sections: slightly non-equilateral triangles for GaN and ribbon-like rectangles for the ZnO. The plane or planes containing the nanowire axis and the oscillatory motion is/are independent of the force distribution because the time-averaged force is nearly zero. These planes are rather determined by the two principal axes

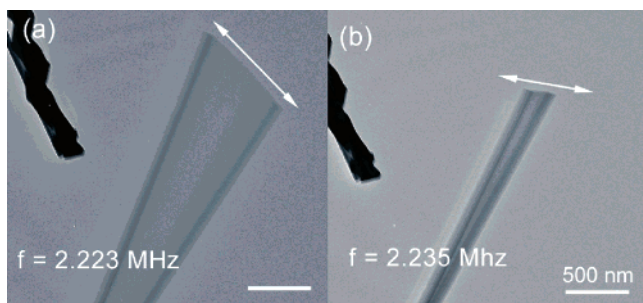


Figure 4. TEM images showing two closely spaced resonances observed in the same wire. The sample was deliberately tilted slightly out of the image plane in order to capture images of both resonance directions by tuning the frequency at fixed tilt angle. (a) Lowest resonance at 2.223 MHz with the bending direction almost perpendicular to the beam axis and (b) slightly higher resonance at 2.235 MHz with bending direction almost parallel to the beam axis. The (orthogonal) planes of both resonant motions contain the nanowire axis. As is obvious from the feature in the upper left corner, the sample orientation (tilt) is the same in both images.

passing through the centroid of the nanowire cross section, along which the moment of inertia, I , is either minimum or

maximum (I_{\min} or I_{\max}).²³ Because the principal axes are orthogonal, the two resonant frequencies depend on the ratio of the (nondegenerate) components of I : $f_o/f'_o = \sqrt{I_{\max}/I_{\min}}$, unless the cross section possesses rotational symmetry higher than twofold, in which case only one frequency is observed.

The three observed f_o/f'_o values in Table 1 are scattered about the ideal value (1.0649) for an isosceles triangle with base angle 58.42° corresponding to our [120]-axis wurtzite nanowires, cf. Figure 1b. This scatter suggests small but significant departures from a perfect isosceles triangle. Only one resonance is observed in the other three nanowires, most likely because the *specific* low-symmetry cross sections of these nanowires are smeared out by more complex morphologies. This, in turn, could result from the development of “extra” facets on the growing nanowire, as suggested by the SEM image in Figure 5a. A more extreme case is Figure 5b where the cross section appears nearly circular, although edges between planar facets are still present. This general idea is supported by cross-sectional TEM studies. A specimen was prepared by focused ion beam (FIB) slicing and lift-out with a micromanipulator. Figure 5c is a bright-field scanning

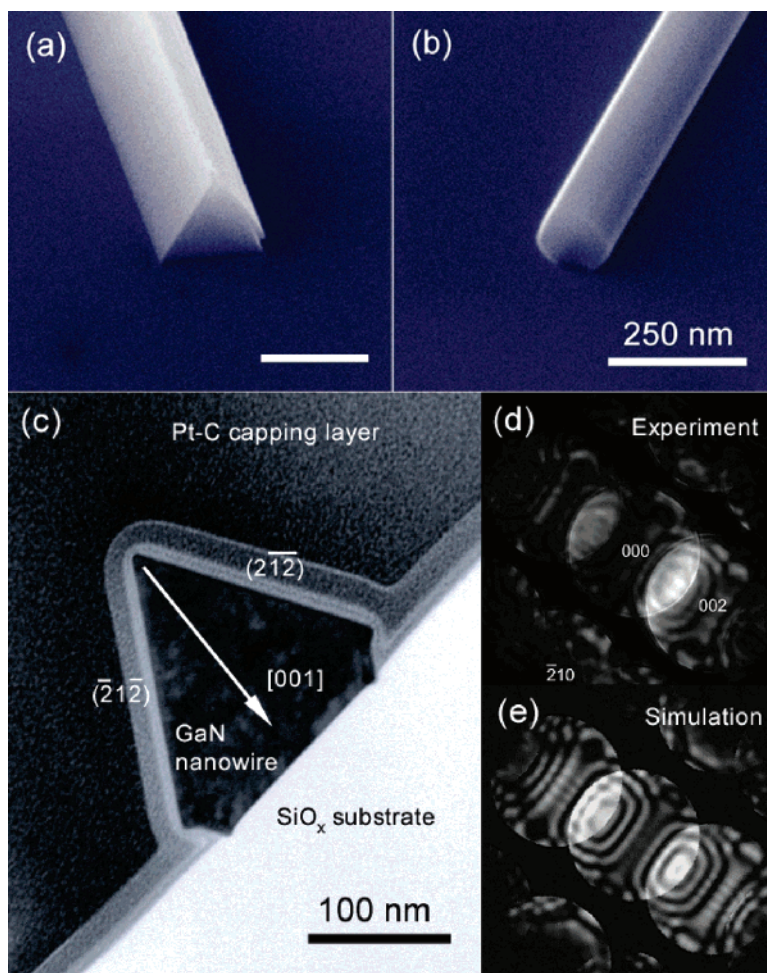


Figure 5. (a and b) SEM image revealing irregular nanowire cross sections. In a, one facet has an extra overgrowth, whereas in b, numerous extra facets give a nearly circular impression. (c) Bright-field STEM image along the [120] growth orientation, showing a third kind of irregular cross section. Here the plane indices and growth orientation were determined from convergent beam electron diffraction (CBED) analysis. (d) Experimental CBED pattern obtained from the nanowire along [120]. (e) Simulated CBED pattern along the [120] direction for a 185-nm-thick GaN thin section specimen confirming the experimental indexing in d.

TEM (STEM) image of a clearly nonisosceles nanowire cross section. Note that [001] in the sample plane is slightly off normal with respect to the base (in contact with the substrate), which therefore subtends nonideal angles with respect to the $(\bar{2}1\bar{2})$ and $(2\bar{1}\bar{2})$ facets. In addition, two small extra facets are developed at the corners of the base. This image was recorded after tilting the specimen such that the electron beam was parallel to the facet edges, thus ensuring that the image represents the actual cross section. Despite the irregular triangular cross section, convergent beam electron diffraction (CBED) analysis (Figure 5d and e) confirmed the nanowire growth orientation as [120], consistent with prior TEM observations. The oddly developed facets are atypical and might be attributed to fluctuations in reaction conditions that affect the stability of growth of a certain plane.³⁷ The uncharacteristically small Q for sample 5 may reflect 2 unresolved closely spaced resonances.

In summary, we measured the diameter-dependent Young's modulus and quality factor of GaN nanowires. For an 84-nm diameter, Young's modulus was close to the theoretical bulk value (~ 300 GPa) but decreased with decreasing diameter. Planar defects running along the wire axis or increasing surface-to-volume ratio were suggested as possible origins. The quality factor was significantly higher than that of conventionally fabricated Si nanowires for a given surface-to-volume ratio, demonstrating the promise of GaN nanowires for NEMS device applications. Finally, moment of inertia considerations combined with cross-sectional TEM and SEM images provide a natural explanation for the observation of oscillatory motions in two orthogonal planes in nanowires with low-symmetry cross sections. Any cross section with less than threefold rotational symmetry will have two orthogonal resonant modes whose frequency ratio depends on the specific cross-sectional shape. This finding could be utilized for the development of advanced GaN nanowire NEMS devices.

Resonance Frequency Determination. In the present capacitively driven resonance experiment, the nanowire resonance occurs when the frequency of the electrostatic force matches the fundamental resonance frequency, f_0 , of the nanowire. If a sinusoidal voltage with frequency f is applied by a function generator ($V = V_0 \sin 2\pi f t$), then the resultant oscillating force has both f and $2f$ terms with amplitudes proportional to V_0 and V_0^2 , respectively, because of the static charges induced by the work function difference between the nanowire and the counter electrode. Resonance thus occurs not only when the drive frequency, f , matches f_0 but also when f matches $f_0/2$ (because the force will have an f_0 term as well as $f_0/2$ when the drive frequency $f = f_0/2$). Between these two drive frequencies, the higher detected frequency should be selected as the true resonance frequency of a nanowire.

Cross-Sectional TEM Sample. The cross-sectional TEM sample is prepared by low-current Ga ion-beam sectioning using the FIB system (FEI DB235) equipped with a micro-manipulator (Ascend Instruments Xtreme Access). An ~ 1 μm thick protective Pt-C layer was first deposited on a segment of nanowire by directly decomposing the Pt orga-

nometallic precursor using the electron beam in the FIB system. An ~ 1 μm thick slab of specimen was sectioned by a high-current Ga ion-beam perpendicular to the nanowire axis. The micromanipulator retrieved the slab, and low-current Ga ion-beam milling was performed until the thickness of the slab was reduced until it was electron-transparent, ~ 100 nm.

Acknowledgment. This research was supported by the US Department of Energy Grant DE-FG02-98ER45701 (C.Y.N.) and the National Science Foundation Grant ECS-0304064 (P.J.). We thank Dr. D. M. Yates for his assistance with electron microscopy. This work utilized central facilities of the Penn Regional Nanotechnology Facility partially supported by the NSF/MRSEC under Grants DMR02-03378 (D.T.) and DMR-0079909 (P.J.).

References

- (1) Nakamura, S.; Fasol, G. *The Blue Laser Diode*; Springer: Berlin, 1997.
- (2) Mishra, U. K.; Parikh, P.; Wu, Y.-F. *Proc. IEEE* **2002**, *90*, 1022.
- (3) Grzegory, I.; Krukowski, S.; Leszczyński, M.; Perlin, P.; Suski, T.; Porowski, S. In *Nitride Semiconductors Handbook on Materials and Devices*; Ruterana, P.; Albrecht, M.; Neugebauer, J., Eds.; WILEY-VCH: Weinheim, Germany, 2003; Chapter 1.
- (4) Shul, R. J.; Vawter, G. A.; Willison, C. G.; Bridges, M. M.; Lee, J. W.; Pearton, S. J.; Abernathy, C. R. *Solid-State Electron.* **1998**, *42*, 2259.
- (5) Beach, R. A.; McGill, T. C. *J. Vac. Sci. Technol., B* **1999**, *17*, 1753.
- (6) Xia, Y.; Yang, P.; Sun, Y.; Wu, Y.; Mayers, B.; Gates, B.; Yin, Y.; Kim, F.; Yan, H. *Adv. Mater.* **2003**, *15*, 353.
- (7) Uenoyama, T. *Phys. Rev. B* **1995**, *51*, 10228.
- (8) Han, W.; Fan, S.; Li, Q.; Hu, Y. *Science* **1997**, *277*, 1287.
- (9) Johnson, J. C.; Choi, H.-J.; Knutsen, K. P.; Schaller, R. D.; Yang, P.; Saykally, R. J. *Nat. Mater.* **2002**, *1*, 106.
- (10) Huang, Y.; Duan, X.; Cui, Y.; Lieber, C. M. *Nano Lett.* **2002**, *2*, 101.
- (11) Zhong, Z.; Qian, F.; Wang, D.; Lieber, C. M. *Nano Lett.* **2003**, *3*, 343.
- (12) Qian, F.; Li, Y.; Gradedecak, S.; Wang, D.; Barrelet, C. J.; Lieber, C. M. *Nano Lett.* **2004**, *4*, 1975.
- (13) Husain, A.; Hone, J.; Postma, H. W. Ch.; Huang, X. M. H.; Drake, T.; Barbic, M.; Scherer, A.; Roukes, M. L. *Appl. Phys. Lett.* **2003**, *83*, 1240.
- (14) Wong, E. W.; Sheehan, P. E.; Lieber, C. M. *Science* **1997**, *277*, 1971.
- (15) Poncharal, P.; Wang, Z. L.; Ugarte, D.; de Heer, W. A. *Science* **1999**, *283*, 1513.
- (16) Jaroenapibal, P.; Luzzi, D. E.; Evoy, S.; Arepalli S. *Appl. Phys. Lett.* **2004**, *85*, 4328.
- (17) Jaroenapibal, P.; Chikkannanavar, S. B.; Luzzi, D. E.; Evoy, S. *J. Appl. Phys.* **2005**, *98*, 044301–1.
- (18) Wang, Z. L.; Gao, R. P.; Pan, Z. W.; Dai, Z. R. *Adv. Eng. Mater.* **2001**, *3*, 657.
- (19) Kim, K.; Lambrecht, R. L.; Segall, B. *Phys. Rev. B* **1994**, *50*, 1502.
- (20) Wright, A. F. *J. Appl. Phys.* **1997**, *82*, 2833.
- (21) Nam, C. Y.; Tham, D.; Fischer, J. E. *Appl. Phys. Lett.* **2004**, *85*, 5676.
- (22) Nam, C. Y.; Kim, J. Y.; Fischer, J. E. *Appl. Phys. Lett.* **2005**, *86*, 193112.
- (23) Meirovich, L. *Element of Vibration Analysis*; McGraw-Hill: New York, 1986.
- (24) Adams R. D.; Bacon, D. G. C. *J. Phys. D: Appl. Phys.* **1973**, *6*, 27.
- (25) Polian, A.; Grimsditch, M.; Grzegory, I., *J. Appl. Phys.* **1996**, *79*, 3343.
- (26) Takagi, Y.; Ahart, M.; Azuhata, T.; Sota, T.; Suzuki, K.; Nakamura, S. *Physica B* **1996**, *219–220*, 547.
- (27) Nowak, R.; Pessa, M.; Suganuma, M.; Leszczynski, M.; Grzegory, I.; Porowski, S.; Yoshida, F. *Appl. Phys. Lett.* **1999**, *75*, 2070.
- (28) Evans, C. C. *Whiskers*; Mills and Boon: London, 1972.
- (29) Schmid, M.; Hofer, W.; Varga, P.; Stoltze, P.; Jacobsen, K. W.; Nørskov, J. K. *Phys. Rev. B* **1995**, *51*, 10937.
- (30) Villain, P.; Beauchamp, P.; Badawi, K. F.; Goudeau, P.; Renault, P.-O. *Scripta Mater.* **2004**, *50*, 1247.

- (31) Branício, P. S.; Rino, J.-P. *Phys. Rev. B* **2000**, *62*, 16950.
- (32) Li, W.; Kalia, R. K.; Vashishta, P. *Europhys. Lett.* **1996**, *35*, 103.
- (33) Tham, D.; Nam, C. Y.; Fischer, J. F., in preparation, 2005.
- (34) Gaspar, J.; Chu, V.; Conde, J. P. *Appl. Phys. Lett.* **2004**, *84*, 622.
- (35) Carr, D. W.; Evoy, S.; Sekaric, L.; Craighead, H. G.; Parpia, J. M. *Appl. Phys. Lett.* **1999**, *75*, 920.
- (36) Bai, X. D.; Gao, P. X.; Wang, Z. L.; Wang, E. G. *Appl. Phys. Lett.* **2003**, *82*, 4806.
- (37) Hiramatsu, K.; Nishiyama, K.; Motogaito, A.; Miyake, H.; Iyechika, Y.; Maeda, T. *Phys. Status Solidi A* **1999**, *176*, 535.

NL051860M